



# Constraining mantle carbon: CO<sub>2</sub>-trace element systematics in basalts and the roles of magma mixing and degassing



Simon Matthews<sup>a,\*</sup>, Oliver Shorttle<sup>a,b</sup>, John F. Rudge<sup>a</sup>, John Maclennan<sup>a</sup>

<sup>a</sup> Department of Earth Sciences, University of Cambridge, Downing Street, Cambridge, CB2 3EQ, United Kingdom

<sup>b</sup> Institute of Astronomy, University of Cambridge, Madingley Road, Cambridge, CB3 0HA, United Kingdom

## ARTICLE INFO

### Article history:

Received 1 July 2017

Received in revised form 24 September 2017

Accepted 25 September 2017

Available online 9 October 2017

Editor: F. Moynier

### Keywords:

mantle  
carbon  
ratios  
degassing  
mixing  
inclusions

## ABSTRACT

Our present understanding of the mantle carbon budget is in part built upon measurements of carbon concentrations in olivine hosted melt inclusions. Only a small number of such datasets are thought to have avoided degassing, having been entrapped prior to CO<sub>2</sub> vapour saturation, and are therefore able to constrain primary CO<sub>2</sub> concentrations. The absence of degassing in melt inclusion datasets has been inferred from the presence of strong correlations between CO<sub>2</sub> and trace elements. In this contribution, we demonstrate that partial degassing followed by magma mixing not only retains such positive correlations, but can enhance them.

Simple models of magma mixing and degassing are used to characterise how CO<sub>2</sub>-trace element systematics respond to CO<sub>2</sub> vapour saturation in primary mantle melts entering the crust, followed by magma mixing. Positive correlations are expected between CO<sub>2</sub> and most trace elements, and the average CO<sub>2</sub>/Ba and CO<sub>2</sub>/Nb ratios are controlled by the pressure of magma storage, rather than the CO<sub>2</sub> concentration in the mantle. We find that the best estimates of mantle CO<sub>2</sub> are the maximum CO<sub>2</sub>/Ba ratios observed in melt inclusion datasets, though a large number of analyses are required to adequately characterise the maximum of the CO<sub>2</sub>/Ba distribution. Using the mixing and degassing models we estimate the number of analyses required to obtain a maximum CO<sub>2</sub>/Ba observation within 10% of the mantle value.

In light of our results, we reassess existing melt inclusion datasets, and find they exhibit systematics associated with partial degassing and mixing. We argue that all the data presently available is consistent with a depleted mantle CO<sub>2</sub>/Ba ratio of ~140, and there is as yet no evidence for heterogeneity in the CO<sub>2</sub>/Ba ratio of the depleted mantle.

© 2017 The Authors. Published by Elsevier B.V. This is an open access article under the CC BY license (<http://creativecommons.org/licenses/by/4.0/>).

## 1. Introduction

The mantle is the largest reservoir by mass in the Earth and through volcanism and subduction remains in continual chemical communication with Earth's atmosphere and oceans. Carbon is a key element in this cycle, providing thermostatic control on Earth's climate via silicate weathering and carbonate subduction (Walker et al., 1981; Hayes and Waldbauer, 2006). Though the concentration of carbon in Earth's mantle is thought to be low (<300 ppm; Javoy and Pineau, 1991; Saal et al., 2002; Cartigny et al., 2008; Michael and Graham, 2015; Le Voyer et al., 2017), the mantle carbon budget may greatly exceed that in any other

reservoir (Cartigny et al., 2008; Hirschmann and Dasgupta, 2009; Dasgupta and Hirschmann, 2010; Dasgupta, 2013; Kelemen and Manning, 2015). In order to understand how the Earth's habitable surface environment was formed and regulated over geological time, the whole-Earth Carbon cycle must be understood (Kasting et al., 1993). The first step in this process is understanding the volatile budgets of major terrestrial reservoirs such as the mantle. Our current understanding is, however, fragmentary due to the scarcity of robust observational constraints on the carbon content of undegassed mantle-derived magmas.

Estimates of the carbon concentration of the depleted mantle are based on a small number of basaltic glass datasets, summarised in Fig. 1, and the CO<sub>2</sub>/<sup>3</sup>He ratio of hydrothermal fluids. Marty (2012) estimate the CO<sub>2</sub> content of the depleted mantle to be 183 ± 92 ppm using a C/<sup>3</sup>He ratio of 2.2 ± 0.6 × 10<sup>9</sup> (Resing et al., 2004) and a <sup>3</sup>He mid-ocean ridge flux of 1000 ±

\* Corresponding author.

E-mail address: [sm905@cam.ac.uk](mailto:sm905@cam.ac.uk) (S. Matthews).

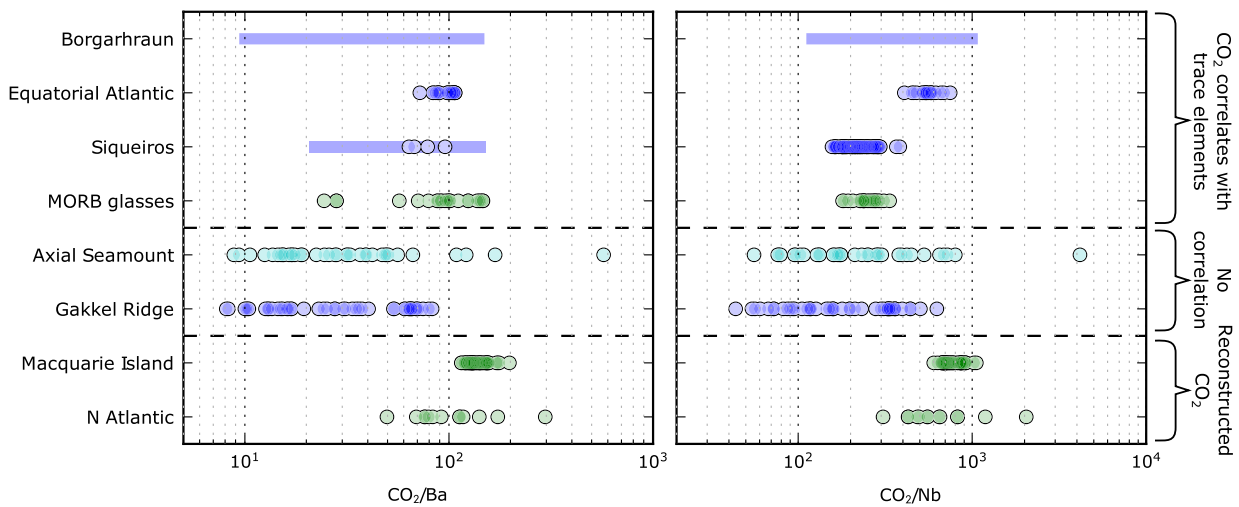


**Fig. 1.** Compilation of published data used for estimating mantle  $\text{CO}_2/\text{Ba}$  and  $\text{CO}_2/\text{Nb}$  ratios. The data are separated into datasets that show a correlation between  $\text{CO}_2$  and trace elements (and have therefore been identified as undegassed on that basis), datasets that show no such correlation (and so have been inferred to be partially degassed), and datasets where the  $\text{CO}_2$  concentration has been reconstructed from Cl concentrations or C-isotope fractionation. Green points indicate data obtained from glasses, cyan points indicate data obtained from plagioclase hosted melt inclusions, and green indicates data obtained from olivine hosted melt inclusions. Bars indicate unpublished data reported by Rosenthal et al. (2015). Data sources: Borgarhraun (Northern Iceland): unpublished data from Hauri et al., reported by Rosenthal et al. (2015); Equatorial Atlantic: Le Voyer et al. (2017); Siqueiros: Saal et al. (2002), unpublished Ba data from Saal et al. reported by Rosenthal et al. (2015); MORB (undersaturated) glasses: Michael and Graham (2015), Shimizu et al. (2016); Axial Seamount: Helo et al. (2011); Gakkel Ridge: Shaw et al. (2010), Wanless et al. (2014); Macquarie Island: Shimizu et al. (2016); N. Atlantic: Cartigny et al. (2008). (For interpretation of the references to colour in this figure legend, the reader is referred to the web version of this article.)

$250 \text{ mol yr}^{-1}$  (Craig et al., 1975). If the mid ocean ridge  $^3\text{He}$  flux is substantially lower, as suggested by Bianchi et al. (2010), the same  $\text{CO}_2/^3\text{He}$  ratio would imply a depleted mantle  $\text{CO}_2$  content of  $\sim 96$  ppm. Primary  $\text{CO}_2$  concentrations in basaltic glasses have been inferred by numerous methods: by correcting for degassing using C isotope fractionation (Cartigny et al., 2008); by using Cl concentrations as a proxy for  $\text{CO}_2$  concentrations (Shimizu et al., 2016); by using maximum values of  $\text{CO}_2/\text{Nb}$  ratios in partially degassed datasets (Shaw et al., 2010; Helo et al., 2011; Wanless et al., 2014); and by looking at the covariation of  $\text{CO}_2$  with Nb or Ba in undegassed suites (Hauri et al., 2002; Saal et al., 2002; Michael and Graham, 2015; Shimizu et al., 2016; Le Voyer et al., 2017). It is this final observational approach that we focus on in this contribution, since undegassed melts provide the most direct constraint on mantle  $\text{CO}_2$  concentrations and their  $\text{CO}_2$ -trace element systematics can additionally provide a probe of the redox state of mantle carbon (Eguchi and Dasgupta, 2017). Basaltic glasses can preserve undegassed  $\text{CO}_2$  either by being entrapped as melt inclusions in growing olivines (Hauri et al., 2002; Saal et al., 2002; Le Voyer et al., 2017), or by having sufficiently low  $\text{CO}_2$  concentrations that they remain undersaturated following eruption (Michael and Graham, 2015; Shimizu et al., 2016). Mantle  $\text{CO}_2$  concentrations inferred from these datasets range from 60–137 ppm. We consider the roles that mixing and degassing may have played in the generation of these glasses, and re-evaluate mantle  $\text{CO}_2$  budgets in light of this.

In order to understand the effects of concurrent magma mixing and degassing on melt inclusion compositions, we use a statistical mixing model combined with simple models for mantle melting and  $\text{CO}_2$  saturation (Section 2). This mixing–degassing model is used to understand the general behaviour of  $\text{CO}_2$ -trace element systematics in Section 3. The implications of these models for the  $\text{CO}_2$  budget and the presence of  $\text{CO}_2$  heterogeneity in the depleted mantle are discussed in Section 4.

### 1.1. Comparing $\text{CO}_2$ to lithophile trace elements

The presence of correlations between  $\text{CO}_2$  and highly incompatible trace elements in suites of co-genetic  $\text{CO}_2$ -undersaturated glasses (Fig. 2), has become an important empirical basis for infer-

ring the behaviour of  $\text{CO}_2$  during mantle melting and degassing. The strong correlation between  $\text{CO}_2$  and Nb in such glass datasets underlies the inference of a close correspondence between the behaviour of  $\text{CO}_2$  and Nb during mantle melting (Saal et al., 2002). This interpretation has been nuanced by recent experimental results, that show that  $\text{CO}_2$  behaves more incompatibly than Nb, having a bulk mantle–melt partition coefficient closer to that of Ba (Rosenthal et al., 2015).

During differentiation and crustal processing, the persistence of correlated enrichments and depletions of incompatible trace elements and  $\text{CO}_2$  is thought to imply that  $\text{CO}_2$  has remained soluble in the melt. Le Voyer et al. (2017) and Saal et al. (2002) identify their melt inclusion suites as being undegassed on this basis. Rosenthal et al. (2015) instead suggest that many of the samples in such co-genetic suites have lost  $\text{CO}_2$ , based on their scatter to low  $\text{CO}_2/\text{Nb}$  ratios (Fig. 2). Understanding the controls on  $\text{CO}_2$ -trace element systematics is therefore vital for assessing if mantle  $\text{CO}_2$ /trace element ratios are reflected in basalts.

### 1.2. The role of mixing in generating trace element systematics

Near-fractional melting of the mantle is expected to generate melts with diverse trace element chemistry. Although considerable variation in trace element concentrations is found in some melt inclusions suites (e.g. Sobolev et al., 1994), it is still significantly less than the diversity predicted from models of fractional melt generation (Kelemen et al., 1997a; MacLennan et al., 2003). In more evolved basaltic matrix glasses, very little variation is preserved (MacLennan, 2008). This decrease in variability with melt evolution has been understood in terms of concurrent mixing and crystallisation (Sobolev, 1996; MacLennan, 2008; Shorttle et al., 2016). The mixing process can efficiently dilute the most incompatible trace-element enriched, and therefore  $\text{CO}_2$  enriched, fractional melts prior to melt inclusion entrapment even in primitive olivine macrocrysts.

Simple statistical models of melt mixing have been able to reproduce many of the observed chemical systematics of melt inclusion and glass suites (Rudge et al., 2013; Shimizu et al., 2016; Shorttle et al., 2016). These models utilise the properties of the Dirichlet distribution to model the geochemical consequences of

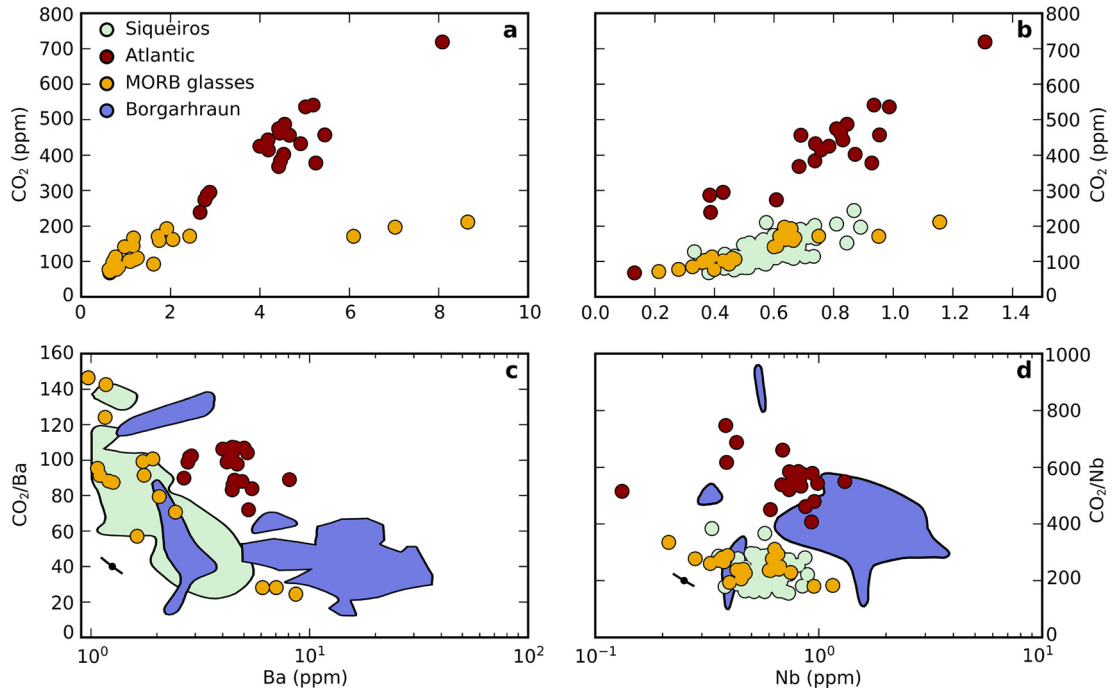


**Fig. 2.** Compilation of Ba, Nb and CO<sub>2</sub> data for mid-ocean ridge melt inclusion and glass datasets reported as being undegassed. Modified from Rosenthal et al. (2015). Data sources: Siqueiros Nb: Saal et al. (2002); Siqueiros Ba: Saal et al. unpublished data reported by Rosenthal et al. (2015); Atlantic: Le Voyer et al. (2017); MORB glasses: Michael and Graham (2015) and Shimizu et al. (2016); Borgarhraun (Northern Iceland): Hauri et al. unpublished data reported by Rosenthal et al. (2015). The black lines and circles in panels c and d show how a 10% uncertainty in Ba or Nb concentration could cause a spurious negative correlation to develop, this effect is much smaller than the signal shown by the datasets. Error in CO<sub>2</sub> measurements will cause vertical displacement of the data points only.

progressive mixing of mantle melts. We build upon such models here, applying them to the creation of volatile element variability in mantle-derived melts and the destruction of this variability by mixing and degassing in the crust.

## 2. Modelling concurrent mixing and degassing

The model comprises three sequential processes, summarised in Fig. 3. Firstly, a melting model for passively upwelling mantle is used to generate the masses and chemistry of fractional melts for a typical mid-ocean ridge (Section 2.1, Fig. 3a). These melts are then placed at a pressure corresponding to magma storage in the crust, and melts that are oversaturated in CO<sub>2</sub> degas until they are in equilibrium (Section 2.2, Fig. 3b). Finally, the melts are partially mixed (Section 2.3, Fig. 3c). We do not attempt to model fractional crystallisation since the melt inclusions preserving primary CO<sub>2</sub>/Nb and CO<sub>2</sub>/Ba ratios represent the most primitive melts.

### 2.1. Melting model

To generate the fractional melts used in the mixing and degassing model, we first calculate the melt fraction extracted,  $X$ , as a function of pressure for passively upwelling mantle using the parameterisation of lherzolite melting by Katz et al. (2003). We set the mantle potential temperature to 1318 °C, a temperature appropriate for normal mid-ocean ridges (Matthews et al., 2016), and cease melting once the base of the crust is reached. A pressure,  $P$ , decrement of 0.006 GPa is used during numerical integration of the melting equations. For computational convenience we then remap the results of these calculations from  $X(P)$  to  $P(X)$ , in steps of equal melt fraction increment (0.01%) using linear interpolation.

The trace element chemistry of the generated melts is calculated assuming near fractional melting, modelled with the equation:

$$C_l = \frac{C_0}{(1 - \Phi)D + \Phi} (1 - X)^{\frac{(1-\Phi)(1-D)}{(1-\Phi)D + \Phi}},$$

(Zou, 2007, equation (3.7)), where  $C_l$  and  $C_0$  are the concentrations of the trace element in the liquid and original solid,  $D$  is the partition coefficient (for simplicity assumed independent of pressure),  $\Phi$  is the residual melt fraction, and  $X$  is fraction of extracted melt. The concentrations of trace elements initially in the solid are set to those in 'Average DMM' of Workman and Hart (2005). The liquid compositions are calculated assuming  $\Phi = 0.5\%$  by mass and  $D$ s appropriate for typical melting conditions of lherzolite (Workman and Hart, 2005). Initial CO<sub>2</sub> concentrations in the melts are calculated in the same manner, assuming a bulk partition coefficient of  $5.5 \times 10^{-4}$  (Rosenthal et al., 2015) and a CO<sub>2</sub>/Ba ratio in the solid of 140, except where noted otherwise.

In these calculations we consider melt generation from a single chemically homogeneous lithology. Though there is evidence for heterogeneity in the depleted mantle, the contribution of melts from heterogeneous domains is likely small (Hirschmann and Stolper, 1996; Matthews et al., 2016). Furthermore, we find melting of a single homogeneous source reproduces the observed CO<sub>2</sub>-trace element systematics adequately. In Appendix C we demonstrate how varying some of the constants used in the melting model affects the statistics described in Section 3.

### 2.2. Degassing model

Once mantle melts have been generated, they may be transported upwards through the mantle in high porosity channels, allowing much of the geochemical variability arising from the melting process to be retained (Spiegelman and Kelemen, 2003). At depths where the melt fraction is not sufficient for high porosity melt channels to form, the melts may become homogenised (Rudge et al., 2013), though this process has only a minor effect on the conclusions drawn here (Appendix A).

Melts can only be preserved in melt inclusions once they have begun to crystallise. Structural and geochemical observations from the Oman ophiolite (Boudier et al., 1996; Kelemen et al., 1997b), and magma storage pressures derived from OPAM

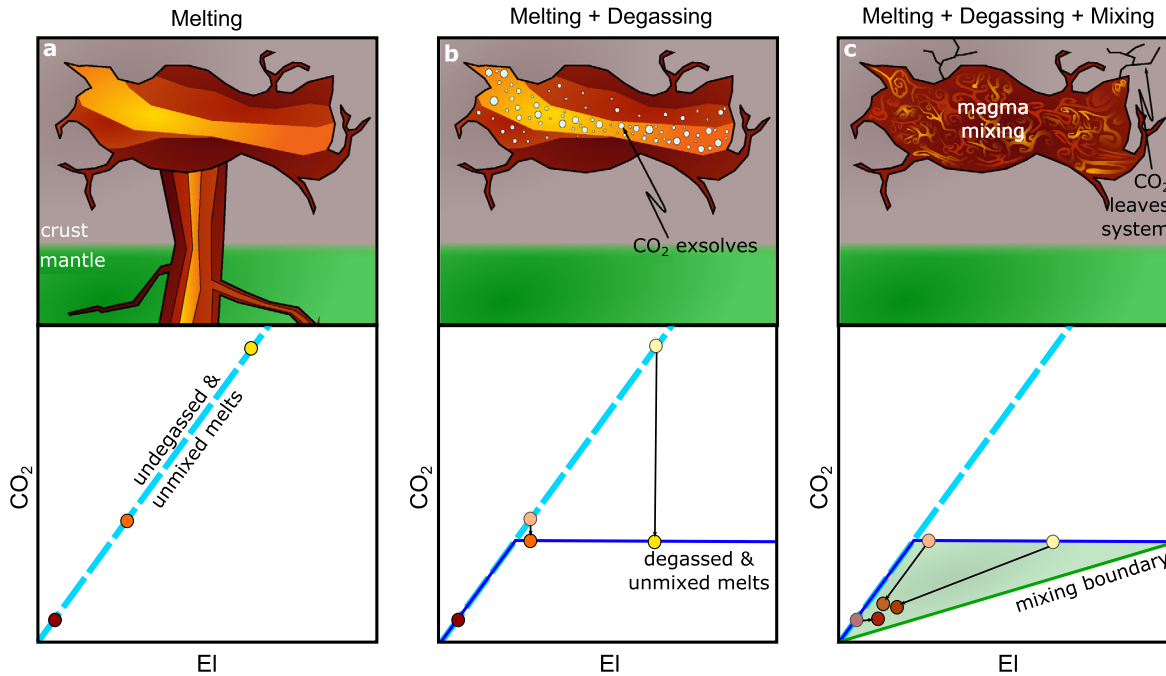


**Fig. 3.** Cartoons showing how the mixing and degassing calculations proceed. 'EI' represents a trace element which behaves identically to CO<sub>2</sub> during mantle melting. In the lower panels, the circles show schematically the behaviour of individual melts throughout the process, whilst the lines show the behaviour of a continuous distribution of melt compositions. The blue dashed line shows the undegassed and unmixed melts (panel a), the solid blue line shows the degassed and unmixed melts (panel b), and the shaded green region (panel c) shows the region between mixing bounds (the solid blue lines and green line). The positions of the solid blue and green lines are determined by the magma storage pressure. (For interpretation of the references to colour in this figure legend, the reader is referred to the web version of this article.)

and clinopyroxene-melt barometry performed on samples from the Icelandic rift zones and mid-ocean ridges (Maclennan et al., 2001; Herzberg, 2004; Winpenny and Maclennan, 2011; Neave and Putirka, 2017), indicate that crystallisation in oceanic rift settings begins beneath the Moho and proceeds to low pressure. This process is shown schematically in Fig. 3a.

The pressure of MORB crystallisation will have a major control on how much of mantle-derived CO<sub>2</sub> variability is preserved in melt inclusions, as pressure is the primary control on CO<sub>2</sub> solubility in basaltic melts (Moore, 1979; Dixon et al., 1995). At the pressures associated with magma storage and crystallisation, even at the Moho, the melts most enriched in CO<sub>2</sub> are likely to be CO<sub>2</sub>-oversaturated. An oversaturated melt will tend to return to saturation by degassing CO<sub>2</sub> (Fig. 3b). To quantify the solubility of CO<sub>2</sub> in the melts, and therefore their variable extents of degassing, we use the solubility model of Shishkina et al. (2014). In addition to modelling the pressure dependence of CO<sub>2</sub> solubility, Shishkina et al. (2014) also quantify the effect of the major element composition of the melt, through a parameter they call  $\pi^*$ . To retain simplicity in our models we set  $\pi^*$  to a constant value of 0.34, typical of mid-ocean ridge tholeiites. In detail,  $\pi^*$  will correlate with trace element concentration, even in melts from a single-lithology mantle, as melt major element chemistry correlates with depth and degree of melting (Klein and Langmuir, 1987). A variable  $\pi^*$  is, however, a secondary effect to the melting and mixing processes we incorporate in our model. We also assume that melts do not retain supersaturation, which means that our results are conservative estimates for the effect of degassing on preserved CO<sub>2</sub>-trace element ratios as some degree of supersaturation is required to drive bubble nucleation (e.g., Bottinga and Javoy, 1990).

A single pressure is chosen for each run of the model, corresponding to the magma storage depth. Melts that have a saturation pressure lower than this retain their initial CO<sub>2</sub> concentration. The most enriched melts may reach CO<sub>2</sub> saturation at greater pressures than the crustal depths used in the models, and therefore may begin degassing before the single degassing stage used in the model.

Since CO<sub>2</sub> solubility monotonically decreases with decreasing pressure, even if these melts lose CO<sub>2</sub> during transport they will in all likelihood still arrive oversaturated in CO<sub>2</sub> at the pressure of magma storage. Degassing during transport will never cause the melts to lose more CO<sub>2</sub> than they would during a single (efficient) degassing interval at the pressure of magma storage. The melts are likely to continue mixing and crystallising as they travel upwards through the crust, and therefore may experience many episodes of degassing followed by mixing. Since the melt inclusions that are most likely to preserve mantle CO<sub>2</sub>/Ba or CO<sub>2</sub>/Nb values are entrapped at the first stage of crystallisation and then remain isolated from the melt, we do not consider subsequent mixing or degassing.

### 2.3. Mixing model

The final step in our model is the mixing of the partially degassed melts generated in the previous two steps (Sections 2.1 and 2.2), shown schematically in Fig. 3c. In making this the last stage of the model, we are implicitly assuming the timescale of degassing, controlled by bubble nucleation, is faster than the timescale of mixing. We follow the statistical mixing methodology used by Rudge et al. (2013) to model the partial mixing process. Rudge et al. (2013) utilise the properties of the Dirichlet distribution, in particular it has very strong independence properties, meaning that all melts are treated equally according to their relative proportions, denoted as  $\omega_i$ . A comprehensive description of the model is given by Rudge et al. (2013), and so we provide only a summary here.

A mixed melt of composition  $\hat{C}$  is generated by randomly mixing  $m$  melt compositions entering the crust,  $C^{(i)}$ , according to their proportions  $\hat{r}_i$ :

$$\hat{C} = \sum_{i=1}^m \hat{r}_i C^{(i)}$$

where the hats on  $\hat{C}$  and  $\hat{r}_i$  indicate that they are random variables. The mean composition of the melts entering the crust is fixed by the mass proportion of each melt present,  $\omega_i$ :

$$\bar{C} = \sum_{i=1}^m \omega_i C^{(i)}$$

therefore, to conform with mass balance the expectation value for the proportions of melts going into a mixture,  $\hat{r}_i$ , is given by:

$$\mathbb{E}(\hat{r}_i) = \omega_i$$

Formally, the proportions that the melts are mixed with are distributed according to a Dirichlet distribution with parameters:

$$\{\hat{r}_1, \hat{r}_2, \dots, \hat{r}_m\} \sim \text{Dir}(\alpha_1, \alpha_2, \dots, \alpha_m)$$

where  $\alpha_i$  is related to the mixing parameter,  $N$ , by:

$$\alpha_i = (N - 1)\omega_i$$

$N$  can range from unity, representing no mixing, to  $\infty$ , representing complete mixing. Melts are weighted by  $\omega_i$  values corresponding to a triangular melting region, i.e. the deepest melts have a greater weighting than more shallow melts. MacLennan (2008) showed that melts in Iceland become increasingly mixed as crystallisation proceeds and the melts become more evolved; Rudge et al. (2013) successfully modelled this by varying the mixing parameter from 12, for the most primitive melts, to 108 for the most evolved. In the models presented here we use a constant mixing parameter of 16, typical of the earliest stages of crystallisation. The effect of the mixing parameter on our results is discussed in Appendix B.

Correlations between  $\text{CO}_2$  and trace elements are a primary consideration of this contribution. The properties of the Dirichlet distribution allow calculation of the variance of individual elements, the covariance of two elements, and from these the Pearson correlation coefficient (Rudge et al., 2013). For melts from a single lithology, as modelled here, the variance of a single element,  $\hat{C}^{(1)}$ , is given by:

$$\text{var}(\hat{C}^{(1)}) = \frac{1}{N} \sum_{i=1}^n \omega_i (c_i^{(1)} - \bar{C}^{(1)})^2$$

and the covariance of two elements,  $\hat{C}^{(1)}$  and  $\hat{C}^{(2)}$ , by:

$$\text{cov}(\hat{C}^{(1)}, \hat{C}^{(2)}) = \frac{1}{N} \sum_{i=1}^n \omega_i (c_i^{(1)} - \bar{C}^{(1)})(c_i^{(2)} - \bar{C}^{(2)})$$

The Pearson correlation coefficient between two elements can be expressed as:

$$\text{cor}(\hat{C}^{(1)}, \hat{C}^{(2)}) = \frac{\text{cov}(\hat{C}^{(1)}, \hat{C}^{(2)})}{\sqrt{\text{var}(\hat{C}^{(1)})\text{var}(\hat{C}^{(2)})}}$$

since the mixing parameter,  $N$ , cancels, the correlation coefficient between two elements is independent of degree of mixing, assuming the remaining range in the element concentrations is significantly above the level of analytical uncertainty.

Whilst it is the correlation between  $\text{CO}_2$  and trace elements that has been used to assess the behaviour of  $\text{CO}_2$  during melting (and whether it has subsequently degassed), the calculation of the mantle  $\text{CO}_2$  concentration assumes direct proportionality between the  $\text{CO}_2$  concentration and  $\text{CO}_2$ /trace element (EI) ratios. The behaviour of  $\text{CO}_2$ /trace element ratios are therefore also of interest. Unfortunately, simple analytical expressions for the variance, covariance and correlation of element ratios at low degrees of mixing do not exist, but can be calculated by drawing a large number

of samples from the Dirichlet distribution. Since the variance of a single element ratio and the covariance of two ratios do not depend on the mixing parameter,  $N$ , in a simple way, the correlation coefficient between element ratios is also a function of mixing parameter (as shown in Appendix B).

### 3. Mixing systematics

Before applying the mixing model, qualitative inferences may be drawn about the covariance and correlation between  $\text{CO}_2$  and trace elements by considering mixing arrays between end member fractional melts. Firstly, the simplest case is characterised: the correlation between  $\text{CO}_2$  and a trace element that behaves identically to  $\text{CO}_2$  prior to  $\text{CO}_2$  vapour saturation (Section 3.1). This approach is then generalised to the correlation between  $\text{CO}_2$  and trace elements with differing compatibility during melting (Section 3.2). Finally, to quantify the correlations between  $\text{CO}_2$  and trace elements, the Dirichlet mixing scheme is introduced in Section 3.2. The implications of mixing for apparent similarities in behaviour of  $\text{CO}_2$  and trace elements are discussed in Section 3.3. In Section 3.4 the control degassing pressure exerts on the resulting  $\text{CO}_2$ -trace element correlations is explored.

#### 3.1. Identical $\text{CO}_2$ -trace element partitioning

If a trace element behaves identically to  $\text{CO}_2$  during mantle melting and crustal differentiation (prior to  $\text{CO}_2$  saturation), concentrations in fractional and variably differentiated melts will describe a straight line passing through the origin when plotted against  $\text{CO}_2$  concentration (Fig. 3a). The most enriched of these fractional melts will be oversaturated in  $\text{CO}_2$  vapour at crustal pressures, and therefore will degas  $\text{CO}_2$  until they reach  $\text{CO}_2$  saturation (Fig. 3b). This degassing process causes the  $\text{CO}_2$  concentrations of the most enriched melts to be decoupled from the trace element concentrations, whilst the depleted melts are unaffected.

Mixing of fractional melts may only produce melt compositions lying within the extremes of the unmixed fractional melts. These bounds may coincide with the arrays of primary fractional melts, otherwise they correspond to mixing lines between extreme compositions (Fig. 3c). Melts generated by mixing of these fractional melts must therefore lie within the green-shaded area on Fig. 3c. When melts originally at  $\text{CO}_2$  vapour saturation mix with undersaturated melts, the mixed melts will become undersaturated, since we do not allow  $\pi^*$  to vary. Mixed melts lying within this triangle will define a positive correlation, with an average  $\text{CO}_2$ /EI ratio that will be considerably lower than the mantle  $\text{CO}_2$ /EI ratio. In the next Section, we explore how differing trace element behaviour affects this observation, and in Section 3.4 we show that the average  $\text{CO}_2$ /EI ratio, even for correlated  $\text{CO}_2$ -EI datasets is controlled primarily by the pressure of degassing.

Though the compositional limits of near-fractional melt mixing can be determined very simply using the process described above, the space enclosed by these limits is not inhabited with uniform likelihood. For extents of melting expected at mid-ocean ridges ( $\leq 15\%$ ), most melts are produced at high melt fractions once the residual mantle has already been almost entirely stripped of incompatible trace elements. Due to the overwhelming proportion of depleted fractional melts, mixed melt compositions are biased towards the depleted region. In the Section 3.2 we quantify this phenomenon with the Dirichlet mixing model.

#### 3.2. Generalised $\text{CO}_2$ -trace element partitioning

The methodology developed in the preceding section can be generalised to elements with differing compatibilities to  $\text{CO}_2$ . The primary melts, rather than falling on a straight array, now define a

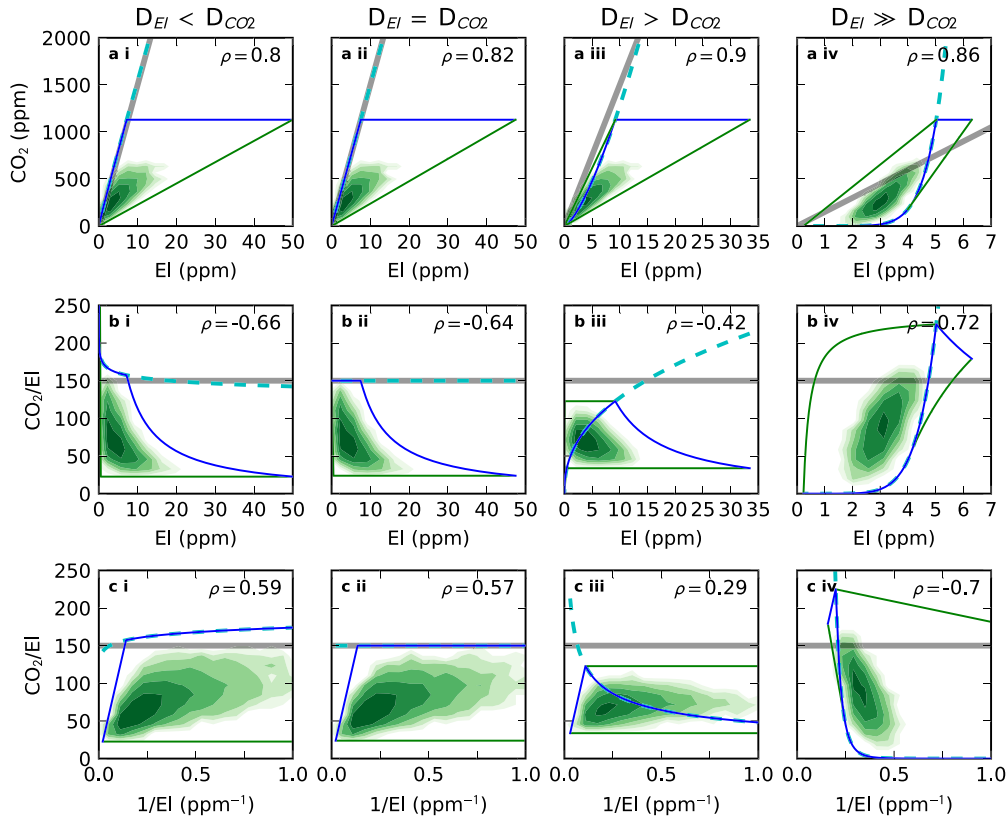


**Fig. 4.** Systematics for trace elements with varying compatibility relative to  $\text{CO}_2$  (column headings) according to our mixing and degassing model. Trace element concentrations in the solid mantle are set to 0.5 ppm. Each row represents a different way of plotting the systematics, as indicated by the axes labels. See Fig. 3 for descriptions of each line. Undegassed and unmixed melts are represented by the cyan dashed line. Degassed and unmixed melts are represented by the solid blue line. The boundaries of the space that can be inhabited by mixed melts are shown by solid green lines, in addition to the solid blue lines. The grey band represents the  $\text{CO}_2/\text{El}$  ratio of the mantle source. The shading represents the logarithmic density of mixed melts generated by the model. The Pearson correlation coefficient ( $\rho$ ) for the mixed distribution is shown in the upper right hand corner of each panel. Calculation parameters are described in the text, the degassing pressure is set to 2 kbar. (For interpretation of the references to colour in this figure legend, the reader is referred to the web version of this article.)

curve (Fig. 4a). Little change from the identical partitioning case is seen for trace elements behaving more incompatibly than  $\text{CO}_2$ , this is due to the residual porosity retained throughout melting, which damps variability in extracted melts when  $D_{\text{El}} < \phi$ . In addition to the systematics in trace element (El)– $\text{CO}_2$  space, we also show the behaviour in  $\text{CO}_2/\text{El}$ –El space (Fig. 4b), and  $\text{CO}_2/\text{El}$ – $1/\text{El}$  space (Fig. 4c). Fig. 4b may be compared with the data compilation in Fig. 2; plotting  $\text{CO}_2/\text{El}$  ratios against  $1/\text{El}$  concentrations offers the advantages of linear mixing bounds and an expansion of the region containing maximum  $\text{CO}_2/\text{El}$  observations (the depleted melts; Fig. 4c).

The green shading in Fig. 4 shows the logarithmic probability distribution of mixed melts, demonstrating that they are biased towards the depleted region of the space, as discussed in Section 3.1. It is immediately apparent from Fig. 4a that positive correlations between  $\text{CO}_2$  and trace elements are generated from partially degassed melts. Importantly, the greatest population density of these melts is seen in a narrow array, similar in appearance (but not gradient) to the expectation from a suite of undegassed melts. This feature persists in spite of the broad mixing bounds (green and blue lines) defined by mixing of endmember melt compositions. The gradient of this array is lower than the  $\text{CO}_2/\text{El}$  ratio of the source (Fig. 4b and Fig. 4c) and the average  $\text{CO}_2/\text{El}$  ratio is much lower than the source  $\text{CO}_2/\text{El}$  ratio (horizontal grey line), although the maximum of the probability distribution does tend towards the source value. In fact, the maximum of the distribution can exceed the source  $\text{CO}_2/\text{El}$  if the trace element is more incompatible (Fig. 4bi), or much more compatible (Fig. 4biv) than  $\text{CO}_2$ . These two scenarios are distinguished from one another by the re-

lation of maximum  $\text{CO}_2/\text{El}$  to El concentration: in the  $D_{\text{El}} \ll D_{\text{CO}_2}$  case,  $\text{CO}_2/\text{El}$  of the melts exceeds the source in the most incompatible trace element depleted melts, whereas for  $D_{\text{El}} \gg D_{\text{CO}_2}$  case, the most incompatible trace element enriched melts have  $\text{CO}_2/\text{El}$  greater than the source. We discuss the implications of this for identifying mantle  $\text{CO}_2/\text{El}$  values in Section 4.3.

$\text{CO}_2/\text{El}$  ratios in melts will only reflect the trace element ratio of the source if  $\text{CO}_2$  has not been fractionated from the trace element. Degassing very strongly fractionates  $\text{CO}_2$  from all trace elements in melts that are oversaturated at the pressure of magma storage, and significantly reduces the  $\text{CO}_2/\text{El}$  ratio of the most enriched melts. Subsequent mixing between the high, primary,  $\text{CO}_2/\text{El}$  ratio of the trace element depleted endmember with the low, degassed,  $\text{CO}_2/\text{El}$  ratio of the trace element enriched endmember, tends to generate negative correlations in  $\text{CO}_2/\text{El}$ –El space (Fig. 4bi–iii) and positive correlations in  $\text{CO}_2/\text{El}$ – $1/\text{El}$  space (Fig. 4ci–iii). Only for the most compatible elements is the original pre-degassing positive correlation of the  $\text{CO}_2/\text{El}$ –El array, or negative correlation for the  $\text{CO}_2/\text{El}$ – $1/\text{El}$  array, retained (Fig. 4biv and Fig. 4civ). Sufficient concentrations of more compatible elements persist in the residue during melting such that many of the higher degree primary melts continue to have significant compatible trace element concentrations, whilst having a primary depletion in  $\text{CO}_2$ . These moderately enriched melts do not saturate in  $\text{CO}_2$  vapour and so retain their primary  $\text{CO}_2/\text{El}$  ratio and therefore continue to provide an enriched high  $\text{CO}_2/\text{El}$  mixing endmember.

Since degassing exerts a control on the systematics of data plotted in  $\text{CO}_2/\text{El}$ – $1/\text{El}$  space, this behaviour can be used to check for and track any degassing processes that a dataset has experienced.

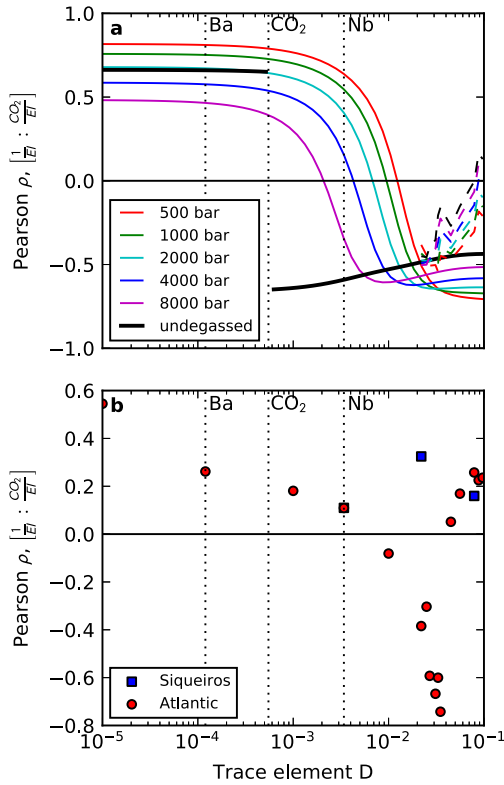


**Fig. 5.** Panel a shows the variation of the Pearson correlation coefficient between  $1/\text{El}$  and  $\text{CO}_2/\text{El}$  calculated for melts mixed following degassing at different pressures. A switch from positive to negative correlation is seen at increasing  $D$  as degassing pressure decreases. Since there is zero variance in  $\text{CO}_2/\text{El}$  for undegassed melts when the trace element partitions identically to  $\text{CO}_2$ , the correlation coefficient is undefined. The trace element  $D$  values are partition coefficients during mantle melting. The vertical dotted lines show the partition coefficients for Ba,  $\text{CO}_2$  and Nb, as reported by Workman and Hart (2005) and Rosenthal et al. (2015). The dashed lines indicate the effect of garnet in the source: trace element concentrations are calculated using the alphaMELTS frontend (Smith and Asimow, 2005) for the pMELTS thermodynamic model (Ghiorso et al., 2002) using variable bulk partition coefficients calculated from constant mineral-melt partition coefficients (McKenzie and O’Nions, 1991, 1995).  $\text{CO}_2$  concentrations were calculated by assuming identical behaviour to Ba. The calculation was run in the CFMAS-Ti system with the depleted mantle composition of Workman and Hart (2005), starting at a temperature of  $1500^\circ\text{C}$  at pressure of 30 kbar (sufficient for garnet to be the stable aluminous phase at the start of melting), and stopped at 2.5 kbar. The trace elements are plotted at the partition coefficients given by Workman and Hart (2005). Panel b shows the Pearson correlation coefficient between  $\text{CO}_2/\text{El}$  and  $1/\text{El}$  for the Equatorial Atlantic dataset (Le Voyer et al., 2017) and the Siqueiros dataset (Saal et al., 2002).

To quantify this behaviour the Pearson correlation coefficient may be used. A coefficient value of 0 indicates no correlation and values of  $-1$  and  $+1$  indicate perfect negative and positive correlations, respectively. The value of the coefficient for the mixed distributions shown in Fig. 4 is displayed in the top right-hand corner of each panel. Fig. 5 shows how correlations in  $\text{CO}_2\text{-El-}1/\text{El}$  space vary with degassing pressure and trace element partitioning coefficient. When there is no degassing (black line), the transition between positive and negative correlations is rapid, and occurs when the trace element switches from being infinitesimally more incompatible, to infinitesimally more compatible than carbon. When partial degassing has taken place a much smoother transition is seen, and correlations cross from negative to positive at progressively greater trace element partition coefficients as the pressure of degassing decreases. Positive correlations are generated by having many low  $\text{CO}_2/\text{El}$  melts at low  $1/\text{El}$  (Fig. 4c), these are the most degassed and incompatible trace element enriched melts. As degassing pressure decreases a greater number of melts degas, and the  $\text{CO}_2$  they retain decreases; the positive correlation will tend to be enhanced. Neg-

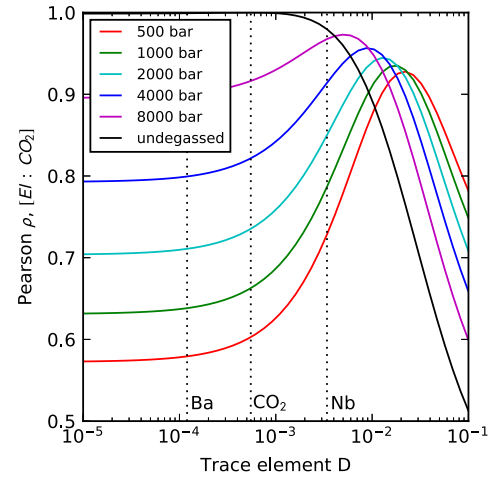


**Fig. 6.** Variation of the Pearson correlation coefficient between concentrations of trace elements of varying partition coefficient during mantle melting ( $D$ ) and  $\text{CO}_2$  concentrations, for different pressures of degassing. When melts have partially degassed the best correlation is seen between  $\text{CO}_2$  and more compatible trace elements. See the caption to Fig. 5 for description of additional lines and data sources.

ative correlations are generated by decoupling between  $\text{CO}_2$  and  $\text{El}$  during melting and so are most prevalent for the most compatible elements. The partition coefficient at which the transition from positive to negative correlation occurs is determined by the competition between these two effects, the tendency to observe a positive correlation in  $\text{CO}_2/\text{El}$  vs.  $1/\text{El}$  space increases with decreasing degassing pressure. The model also makes predictions about the variance in  $\text{CO}_2/\text{El}$  with  $\text{El}$  concentration, however existing datasets do not contain sufficient analyses to accurately estimate these parameters and allow us to test the model.

### 3.3. Apparent mantle partitioning behaviour from $\text{CO}_2$ -trace element correlations

Empirical constraints have been placed on the partitioning behaviour of  $\text{CO}_2$  during mantle melting by the degree of correlation between  $\text{CO}_2$  and trace elements (Saal et al., 2002; Michael and Graham, 2015; Le Voyer et al., 2017). Saal et al. (2002) and Michael and Graham (2015) find the strongest correlation between  $\text{CO}_2$  and Nb, whilst Le Voyer et al. (2017) find  $\text{CO}_2$  correlates equally well with Rb, Ba and Nb. Such relationships between carbon and trace elements only directly reflect mantle partitioning behaviour if no degassing has occurred, with the results above showing that positive correlations are readily generated in partially degassed melts (Fig. 4).

The behaviour of the correlation coefficient between  $\text{CO}_2$  and trace elements as a function of partition coefficient is displayed in Fig. 6. When there is no degassing,  $\text{CO}_2$  correlates extremely well with the most incompatible elements; the lack of variation in correlation coefficient for the most incompatible elements arises from the residual porosity during melting (i.e., our use of a continuous melting model as opposed to pure fractional). The correlation coefficient between  $\text{CO}_2$  and trace elements then decreases with increasing trace element compatibility (Fig. 6, black line).

In contrast, when partially degassed melts are mixed, the correlation coefficient does not decrease monotonically as the reference trace element becomes increasingly compatible. Instead, mixing of degassed melts creates a maximum in correlation coefficient centred on a higher (i.e. more compatible) partition coefficient than  $\text{CO}_2$  (Fig. 6). This pattern is also present in the synthetic data presented in Fig. 4a, which shows data lying within a tight wedge. This result owes to a smaller range in trace element concentrations being generated when the trace element  $D$  is high. Model runs

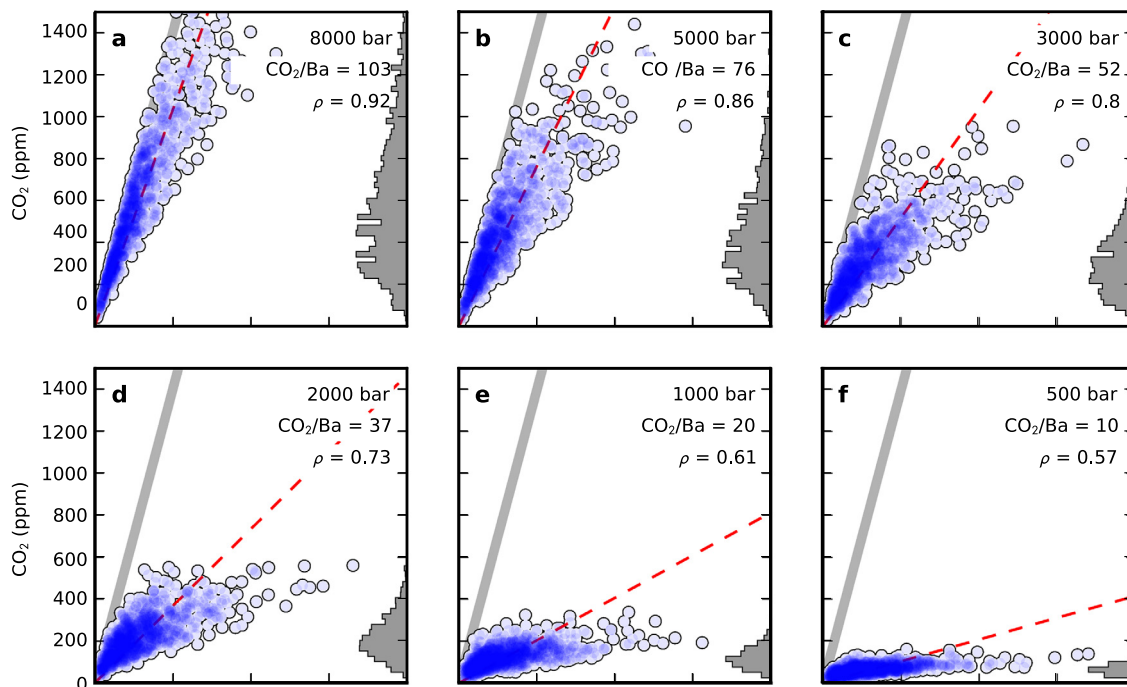


**Fig. 7.** Each panel displays the  $\text{CO}_2$ -Ba systematics generated by mixing melts degassed at different pressures (shown in bar, in the upper right corner). As the degassing pressure decreases, the array of melt compositions rotates to lower  $\text{CO}_2/\text{Ba}$ . Histograms of mixed melt density shown on the right hand side. The shading indicates density of data. The thick grey line shows the  $\text{CO}_2/\text{Ba}$  ratio of the source mantle (140), and the red-dashed line the  $\text{CO}_2/\text{Ba}$  ratio obtained by orthogonal distance regression on the mixed melts (also shown in the top right hand corner of each panel). (For interpretation of the references to colour in this figure legend, the reader is referred to the web version of this article.)

shown in Fig. 7, where  $\text{CO}_2$  is plotted against Ba, and Fig. 8, where  $\text{CO}_2$  is plotted against Nb, show how better correlations may be developed between  $\text{CO}_2$  and Nb, rather than  $\text{CO}_2$  and Ba, despite the carbon partition coefficient used in the models being closer in value to Ba (Rosenthal et al., 2015).

### 3.4. Effect of degassing pressure

The  $\text{CO}_2/\text{El}$  ratios of the melts generated by the model are controlled by mixing between a trace element depleted, but high, primary,  $\text{CO}_2/\text{El}$  endmember, and a trace element enriched, but low, degassed,  $\text{CO}_2/\text{El}$  endmember. The value of the low  $\text{CO}_2/\text{El}$  endmember is determined by the  $\text{CO}_2$  content of the melts at saturation, which is controlled by pressure. Reducing the pressure of degassing has the effect of rotating the array in  $\text{CO}_2$ -trace element space to shallower slopes (Fig. 7 and Fig. 8).

The mantle  $\text{CO}_2/\text{Nb}$  ratio has often been constrained by fitting a line through the data in  $\text{CO}_2$ -trace element space. This process should be carried out using orthogonal distance regression, since neither variable is strictly dependent. We fit an equation of the form:

$$f(\text{El}) = m \cdot \text{El}$$

where El is the concentration of the trace element, and  $m$  is varied so that the misfit between  $\text{CO}_2$  and  $f(\text{El})$  is minimised. The parameter  $m$  corresponds to the best fit  $\text{CO}_2/\text{El}$  ratio. Calculations were performed using the ODRPACK library (Brown and Fuller, 1990) with the SciPy interface (Jones et al., 2014). The results of these calculations are shown by the red dashed lines in Fig. 7 and Fig. 8, and the values of the best fit  $\text{CO}_2/\text{El}$  ratio are shown in the top right corner of each panel. Any amount of degassing reduces the  $\text{CO}_2/\text{El}$  ratio inferred by this method, despite an apparently good fit to the data in  $\text{CO}_2$ -trace element space. As the number of draws from the distribution increases, the best fit ratio will tend towards the mean ratio of the starting melts.

### 3.5. Effect of analytical uncertainty

Using plots where one variable appears in the expressions plotted on both  $x$  and  $y$  axes can lead to the appearance of spurious correlations (Jackson and Somers, 1991). Analytical error in El concentration will not only affect the concentration of El (or  $1/\text{El}$ ) plotted on the  $x$  axis, but also the value of  $\text{CO}_2/\text{El}$  plotted on the  $y$  axis. Measurements of trace element and  $\text{CO}_2$  concentrations in melt inclusions generally have uncertainties  $\sim 10\%$  (Saal et al., 2002; Le Voyer et al., 2017), the vector that describes the effect of this uncertainty is shown by the black lines and circles in Fig. 2c and 2d. In the datasets considered here the signal is much greater than the analytical uncertainty.

## 4. Implications for existing datasets

In Section 3.2 we demonstrated that positive correlations between  $\text{CO}_2$  and trace elements are not a unique property of undegassed melts. Published datasets that have utilised the presence of  $\text{CO}_2$ -trace element correlations as a criterion for identifying the absence of degassing must, therefore, be reassessed.

### 4.1. Signatures of partial degassing in nominally undegassed sample suites

Since degassing only affects the melts that have the highest concentrations of  $\text{CO}_2$ , additional structure is introduced into the data: rather than almost horizontal arrays in  $\text{CO}_2/\text{Ba}$ -Ba space, partially degassed melts will exhibit negative correlations. Fig. 2c demonstrates that the data from Siqueiros, Northern Iceland, Equatorial Atlantic and the undersaturated D-MORB glasses all exhibit these negative correlations between  $\text{CO}_2/\text{Ba}$  and Ba. Furthermore, if  $\text{CO}_2$  has not degassed prior to inclusion entrapment, the correlation coefficient between  $\text{CO}_2/\text{El}$  and  $1/\text{El}$  should reverse sign as trace elements go from being more incompatible to more compatible than  $\text{CO}_2$  during melting (Fig. 5). The data from both Siqueiros



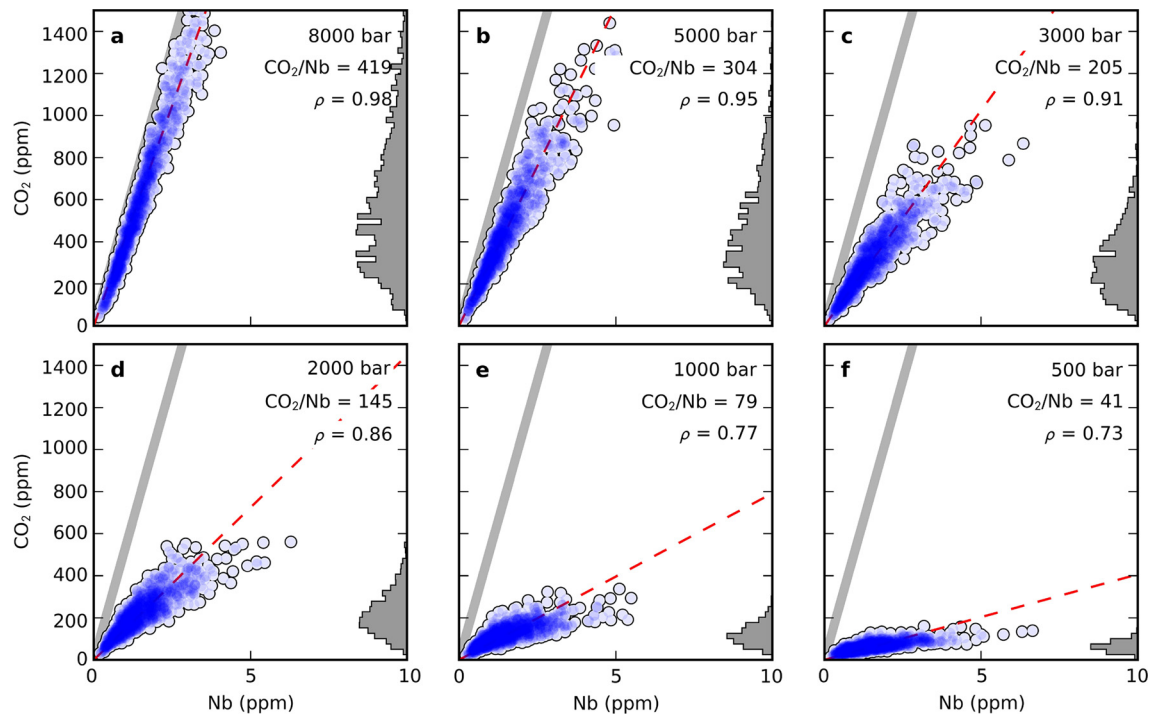


**Fig. 8.** Each panel displays the CO<sub>2</sub>–Nb systematics generated by mixing melts degassed at different pressures (shown in bar, in the upper right corner). As the degassing pressure decreases, the array of melt compositions rotates to lower CO<sub>2</sub>/Nb, but with better correlations than seen for CO<sub>2</sub> and Ba (Fig. 7). Histograms of mixed melt density shown on the right-hand side. The shading indicates density of data. The thick grey line shows the CO<sub>2</sub>/Nb ratio of the source mantle (531), and the red-dashed line the CO<sub>2</sub>/Nb ratio obtained by orthogonal distance regression on the mixed melts (also shown in the top right hand corner of each panel). The CO<sub>2</sub> concentration in the mantle source is identical to that used in the calculations shown in Fig. 7. (For interpretation of the references to colour in this figure legend, the reader is referred to the web version of this article.)

and Equatorial Atlantic retain a positive correlation far beyond the experimental CO<sub>2</sub> partition coefficient (Rosenthal et al., 2015), and beyond Nb which CO<sub>2</sub> has been likened to empirically (Saal et al., 2002). This decoupling between the apparent partition coefficients of CO<sub>2</sub> and trace elements in all these datasets also suggests that they have experienced partial degassing.

At higher values of trace element D, the correlation coefficients between CO<sub>2</sub>/El and 1/El calculated from the published data departs from the predicted behaviour (Fig. 5b). This departure is likely to arise from the behaviour of these elements during garnet-field melting or fractional crystallisation. When garnet is in the residue, the bulk partition coefficients during mantle melting increase significantly. This variation can be modelled with the alphaMELTS frontend (Smith and Asimow, 2005) to the pMELTS thermodynamic model (Ghiorso et al., 2002), and the resulting correlations are shown in Fig. 5 (dashed lines, calculation details given in figure caption). Garnet-field melting can account for this discrepancy, though we do not rule out the role of fractional crystallisation.

The undersaturated glass dataset, shown in Figs. 1 and 2, displays CO<sub>2</sub> co-variation with both Ba and Nb; additionally, and a negative correlation between CO<sub>2</sub>/Ba and Ba. These properties are consistent with the partial degassing and mixing model despite the dataset not representing co-genetic melts. The partial degassing and mixing process may still be controlling the systematics of this dataset if the glasses are derived from melts sampling sources with the same CO<sub>2</sub>/Ba, but with different proportions of low and high degree melts, and mixing occurring at similar pressures. Whilst this uniformity is not ubiquitous in the global mid-ocean ridge system, it may well be present when only undersaturated glasses are considered. Alternatively, varying mantle Ba concentration, at near-constant CO<sub>2</sub> concentration, could generate the observed co-variation between CO<sub>2</sub>/Ba and Ba concentrations in the glasses.

Previous studies have interpreted melt inclusions from the Siqueiros fracture zone to be near primary melts, having undergone negligible mixing and fractionation within the crust (Perfit et al., 1996). However, the CO<sub>2</sub>–trace element systematics are difficult to explain without the partial degassing and mixing processes. The Siqueiros melts are very depleted in trace elements. Furthermore, whilst the trace element data might be matched by batch melting models, it does not preclude their origin from mixing of more variable fractional melts. U-Series disequilibria provide support for fractional melting, indicating that Siqueiros fracture zone melts segregated from their residue at small porosities in a process that must therefore have been near-fractional (Lundstrom et al., 1999). Recent seismic evidence suggests axial magma chambers are present beneath ultra-slow spreading ridges (Jian et al., 2017). Therefore, despite the lower rates of magma supply, these slow spreading systems nonetheless retain melt that new primitive magmas may interact with during their transport and storage in the crust.

#### 4.2. Global mantle CO<sub>2</sub> heterogeneity

Substantial heterogeneity in the CO<sub>2</sub>/Nb and CO<sub>2</sub>/Ba ratios of the depleted mantle has been inferred from the variation in averages of these ratios, obtained by fitting lines through data in CO<sub>2</sub>–Ba and CO<sub>2</sub>–Nb space from Siqueiros, Northern Iceland and the Equatorial Atlantic. For the reasons outlined above, the inclusions measured in these studies are all likely to be preserving partially degassed melts. When partial degassing and mixing has taken place the apparent ratio in CO<sub>2</sub>–Ba and CO<sub>2</sub>–Nb space is determined not by the primary mantle ratios, but by the degassing pressure (Section 3.4). Instead, the best estimate of mantle CO<sub>2</sub> concentration comes from the maximum ratio CO<sub>2</sub>/Ba ratio recorded by the most trace element depleted melts in the dataset; these melts are the most likely to have remained CO<sub>2</sub>

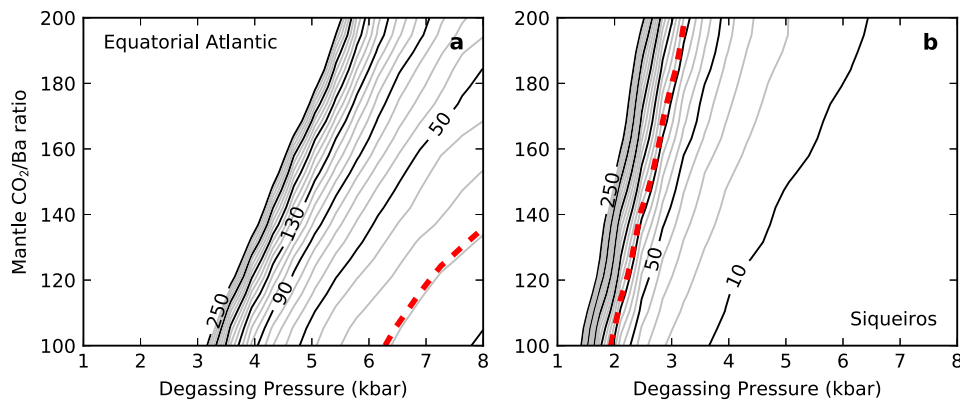


**Fig. 9.** Contours of the minimum number of analyses required to get at least one analysis (in all of 500 model runs) recording a  $\text{CO}_2/\text{Ba}$  ratio within 10% of the mantle value, as a function of degassing pressure and mantle  $\text{CO}_2/\text{Ba}$  ratio. Contours are spaced at intervals of 10 analyses. In panel a the melting model described in Section 2.1 is used and is appropriate for the comparison to the Equatorial Atlantic dataset (Le Voyer et al., 2017), which contains 21 melt inclusion analyses, indicated by the thick red dashed line. Panel b uses a similar melting model, but with a mantle Ba concentration typical of the D-MORB source (Workman and Hart, 2005), and is appropriate for comparison with the Siqueiros dataset (Saal et al., 2002), which contains 97 analyses. In both panels the mixing parameter is set to  $N = 16$ . (For interpretation of the references to colour in this figure legend, the reader is referred to the web version of this article.)

undersaturated (Section 3.2). The maximum  $\text{CO}_2/\text{Ba}$  ratios observed in melt inclusions from Siqueiros and Northern Iceland, and the undersaturated D-MORB glasses, are all  $\sim 140$  (with a maximum value of 146). If this observed maximum ratio is close to the real maximum of the distributions of mixed melts, then it suggests all three datasets are consistent with a single depleted mantle  $\text{CO}_2/\text{Ba}$  ratio. Furthermore, apart from one extreme outlier, the maximum  $\text{CO}_2/\text{Ba}$  ratios in melt inclusions from Axial Seamount (Helo et al., 2011) and Gakkel Ridge (Shaw et al., 2010; Wanless et al., 2014) are consistent with this (Fig. 1). In contrast, the maximum  $\text{CO}_2/\text{Ba}$  ratio observed in the Equatorial Atlantic melt inclusions is 107. This could be reconciled either by the Equatorial Atlantic dataset not adequately characterising the maximum  $\text{CO}_2/\text{Ba}$  ratio in the distribution, or by localised mantle  $\text{CO}_2/\text{Ba}$  heterogeneity as might be expected given the presence of Ba/Nb heterogeneity in the MORB source (Michael and Graham, 2015). Though small-scale mantle heterogeneity has been observed in both the MORB and Iceland mantle sources, linking this to volatile elements such as carbon is intrinsically difficult owing to a bias in preserving the  $\text{CO}_2/\text{Ba}$  ratios of only the most depleted melts.

An alternative possibility to the model we have developed here is that diversity in melt  $\text{CO}_2/\text{Ba}$  and  $\text{CO}_2/\text{Nb}$  arises from mantle  $\text{CO}_2/\text{Ba}$  and  $\text{CO}_2/\text{Nb}$  heterogeneity. Melting of such a heterogeneous mantle must produce both a high  $\text{CO}_2/\text{Ba}$ , low Ba component, and a low  $\text{CO}_2/\text{Ba}$ , high Ba component. For the observed negative correlations between  $\text{CO}_2/\text{Ba}$  and Ba to be generated, a low  $\text{CO}_2/\text{Ba}$ , low Ba component cannot be involved in mixing. However, generating such melts is a natural consequence of melting mantle heterogeneities beyond the smallest of melt fractions, at which point even enriched lithologies are depleted in highly incompatible elements such as Ba. Therefore, mantle heterogeneity alone is highly unlikely to account for the observed correlations.

#### 4.3. Constraining mantle $\text{CO}_2/\text{Ba}$

In a partially degassed dataset, the  $\text{CO}_2/\text{Ba}$  measurement most likely to represent the mantle  $\text{CO}_2/\text{Ba}$  ratio is the maximum ratio observed. A disadvantage of utilising maxima in geochemical datasets is that they are strongly dependent on sample size. For melts to preserve high  $\text{CO}_2/\text{Ba}$  they must have minimal interaction with degassed melts. Depending on the diversity of melts entering magma storage regions, only a small proportion of melts may retain their primary  $\text{CO}_2/\text{Ba}$ . It is therefore most pragmatic to consider the likelihood of melts retaining a  $\text{CO}_2/\text{Ba}$  ratio within 10% of the mantle value.

Fig. 9 shows the minimum number of melt inclusion analyses (or here, Dirichlet distributed draws from a population of synthetic melts) required for the maximum  $\text{CO}_2/\text{Ba}$  ratio measured to be within 10% of the mantle value (with  $>99.8\%$  certainty), for a melting column typical of normal mid-ocean ridges. Since Siqueiros has been identified as sampling ultra-depleted mantle, Fig. 9b demonstrates how the minimum number of analyses changes if trace element concentrations are more depleted in the mantle source (Workman and Hart, 2005). At constant source  $\text{CO}_2/\text{Ba}$  ratio, a source more depleted in trace elements will produce melts that are, on average, less  $\text{CO}_2$  rich, and therefore more likely to retain their primary  $\text{CO}_2/\text{Ba}$  ratio. The number of analyses required increases as degassing pressure decreases and mantle  $\text{CO}_2/\text{Ba}$  increases; both these changes cause the proportion of melts degassing  $\text{CO}_2$  to increase, therefore increasing the likelihood of an undegassed melt mixing with degassed melt and thus erasing the signal of primary  $\text{CO}_2/\text{Ba}$  from the population of melts. In addition, the value of the mixing parameter will affect the position of the contours in Fig. 9, with greater degrees of mixing making observing mantle  $\text{CO}_2/\text{Ba}$  less likely. Making large numbers of analyses on melt inclusions trapped at high pressure offers the greatest prospect of observing the mantle  $\text{CO}_2/\text{Ba}$  ratio.

Both the Borgarhraun and Siqueiros datasets consist of around 100 melt inclusion analyses each (Fig. 9a). Provided these inclusions were trapped at sufficient pressure, the maximum  $\text{CO}_2/\text{Ba}$  they record is likely to be very close to the mantle value. However, the Mid-Atlantic dataset consists of 21 melt inclusion analyses only (Fig. 9a). Barometry indicates crystallisation takes place at pressures as high as 10 kbar beneath the Mid-Atlantic ridge, though erupted liquids predominantly equilibrate at lower pressures (Herzberg, 2004). If the Mid-Atlantic dataset is also sampling a mantle of  $\text{CO}_2/\text{Ba} = 140$ , Fig. 9 suggests the maximum observed  $\text{CO}_2/\text{Ba}$  ratio will only preserve the mantle value if inclusions were entrapped at the deepest extents of crystallisation ( $>8$  kbar). Therefore, the Mid-Atlantic dataset may also be consistent with a mantle  $\text{CO}_2/\text{Ba}$  ratio of 140.

Assuming a Ba concentration in the depleted mantle of 0.563 ppm (Workman and Hart, 2005), a  $\text{CO}_2/\text{Ba}$  ratio of 140 ppm implies a mantle  $\text{CO}_2$  content of 79 ppm, more than double that inferred by Workman and Hart (2005) from the canonical  $\text{CO}_2/\text{Nb}$  ratio (Saal et al., 2002). Rosenthal et al. (2015) reach a similar conclusion, and also discuss the likely  $\text{CO}_2$  content of mantle melting beneath intra-plate volcanoes.

#### 4.4. Origin of CO<sub>2</sub> undersaturation

Both the Siqueiros melt inclusions and undersaturated mid-ocean ridge glass datasets record CO<sub>2</sub> concentrations that are undersaturated at the pressure of eruption, and the CO<sub>2</sub> concentrations present in the Equatorial Atlantic dataset would be undersaturated at during crystallisation within the oceanic crust. This CO<sub>2</sub> undersaturation has been used as further evidence for the absence of degassing (Saal et al., 2002; Michael and Graham, 2015). Though the mixing–degassing model requires some of the fractional melts to become CO<sub>2</sub> saturated, they subsequently mix with highly CO<sub>2</sub> undersaturated melts, resulting in all melts becoming undersaturated at the pressure of degassing (Fig. 7). If a sufficient mass of depleted melts are present, this undersaturation may be retained at the pressure of eruption, as in the Siqueiros and undersaturated mid-ocean ridge glass datasets, even with mixing in of enriched low CO<sub>2</sub>/En melts having occurred.

#### 5. Conclusions

CO<sub>2</sub> concentrations in melt inclusions provide an important constraint on global CO<sub>2</sub> flux from the mantle at mid-ocean ridges and ocean islands and are vital for assessing CO<sub>2</sub> heterogeneity in the mantle. Melt inclusion datasets are a key petrological tool for addressing these problems, and in this study we have formalised the robustness of the melt inclusion archive to the common magmatic processes of mixing and degassing.

We have identified how trace elements co-vary with CO<sub>2</sub> in melts, following mixing of trace element depleted CO<sub>2</sub> undersaturated melts with trace element enriched CO<sub>2</sub> saturated melts. We show that when degassing occurs, CO<sub>2</sub> may have a stronger correlation with Nb, even if its partitioning behaviour during melting is more similar to Ba (Rosenthal et al., 2015). We find that the average CO<sub>2</sub>/Ba ratio in a melt inclusion dataset is dominated by the pressure of degassing, rather than the mantle CO<sub>2</sub>/Ba ratio.

The best estimate of mantle CO<sub>2</sub>/Ba ratio is, instead, the maximum CO<sub>2</sub>/Ba ratio observed.

Comparison of the model results with CO<sub>2</sub>-undersaturated D-MORB glasses (Michael and Graham, 2015), and melt inclusion datasets from Northern Iceland (Hauri et al., 2002), Siqueiros (Saal et al., 2002) and the Equatorial Atlantic (Le Voyer et al., 2017), suggests these datasets all record CO<sub>2</sub> concentrations generated by mixing of partially degassed melts (Section 4). We argue that the available datasets are all consistent with a depleted mantle CO<sub>2</sub>/Ba of ~140, and do not require heterogeneity in mantle CO<sub>2</sub>/Ba.

The role of mixing in the generation of melts trapped in melt inclusions has been neglected in the interpretation of CO<sub>2</sub> concentrations, leading to underestimation of the CO<sub>2</sub> content of the mantle and inferences of CO<sub>2</sub> heterogeneity. Despite the likely presence of partial degassing in all melt inclusion datasets, fully characterising the maxima of CO<sub>2</sub>/Ba values by making many melt inclusion analyses may allow the mantle CO<sub>2</sub>/Ba ratio to be extracted from the data. Subject to the assumptions of our simple melting and mixing models, we can estimate the likelihood of recovering mantle CO<sub>2</sub>/Ba in melt inclusion datasets, a result which is useful in preparing analytical studies.

#### Acknowledgements

The authors would like to thank the Isaac Newton Institute for Mathematical Sciences for its hospitality during the programme ‘Melt in the Mantle’, which was supported by EPSRC Grant Number EP/K032208/1. SM was supported by a Natural Environment Research Council Studentship NE/L002507/1 and NE/M000427/1. OS thanks Trinity College Cambridge for support through a Title A Fellowship. JFR thanks the Leverhulme Trust. Raj Dasgupta and an anonymous reviewer are thanked for their constructive comments which helped improve the manuscript. Frederic Moynier is thanked for his editorial handling.

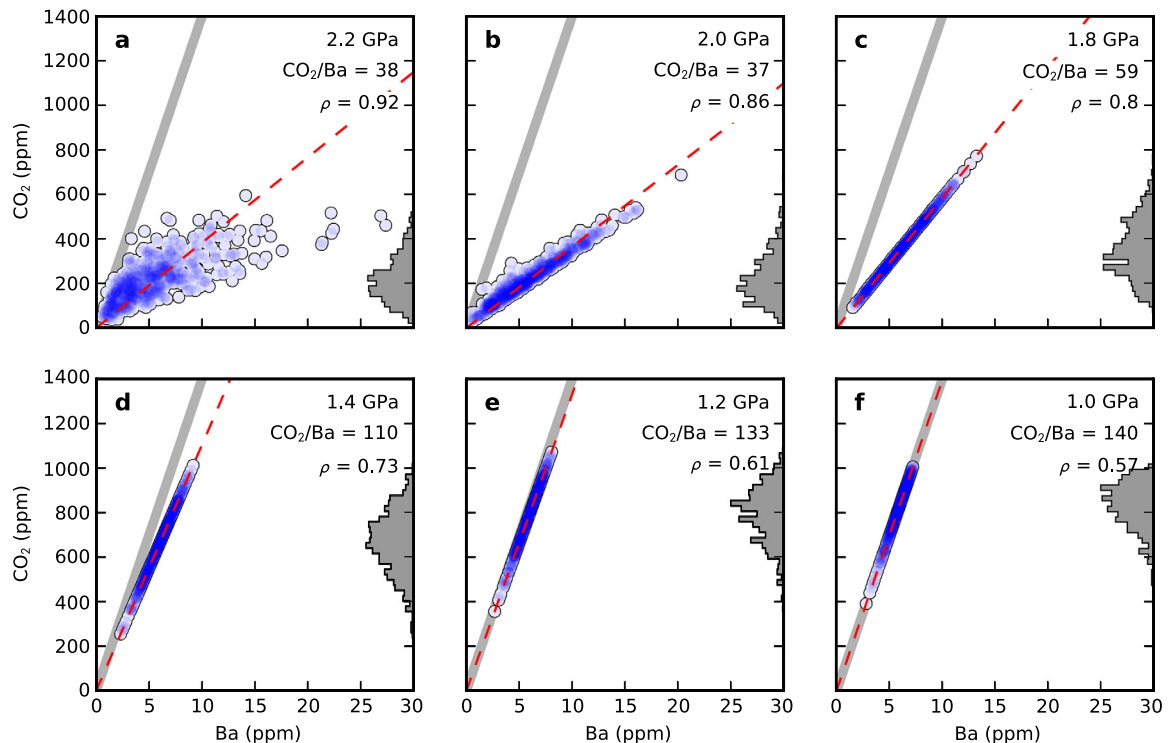


**Fig. A.1.** Each panel shows the results of the mixing–degassing calculation for melts that have been variably homogenised during transport. As the extent of homogenisation increases, the variability in the CO<sub>2</sub>/Ba ratio decreases, and the array rotates towards the mantle CO<sub>2</sub>/Ba ratio. The pressure in the upper-right corner of each panel shows the pressure below which all melts produced are completely mixed. Degassing occurred at 2000 bar. See Fig. 7 for more information.

## Appendix A. Effect of homogenisation during transport on CO<sub>2</sub>-trace element systematics

Soon after mantle crosses the peridotite solidus, the melt fraction will be low and the high porosity melt channels, thought to be critical in preserving primary melt variability, may be yet to form. Melts may therefore homogenise at these depths, Rudge et al. (2013) find such a process is required for subsequent melt mixing to produce the binary isotope arrays observed in Iceland.

The effect of this process, with varying homogenisation depth, is shown in Fig. A.1. As the homogenisation depth increases more melts are mixed together, and the variability of the melts entering the crust is reduced. At the greatest extents of homogenisation (Panels e and f), the extremely high concentrations of CO<sub>2</sub> in the deepest melts is sufficiently diluted by the addition of shallower

melts that CO<sub>2</sub> saturation is no longer reached; the melts preserve the mantle CO<sub>2</sub>/Ba ratio. At more modest extents of homogenisation (Panels c and d), the variability in CO<sub>2</sub> concentration has been removed, but the deepest melts are not sufficiently diluted that they do not saturate in CO<sub>2</sub> in the crust; binary mixing now takes place between a trace element enriched degassed melt, and an extremely depleted undegassed melt, and the mantle CO<sub>2</sub>/Ba ratio is not preserved. When only limited homogenisation takes place (Panel b), the variability of melts is reduced but not sufficiently for a binary mixing array to be produced; the scatter about the average ratio is considerably less than the unhomogenised case (Panel a), however.

Since binary mixing arrays in CO<sub>2</sub>-trace element space are not observed in the published datasets, it is likely that only limited

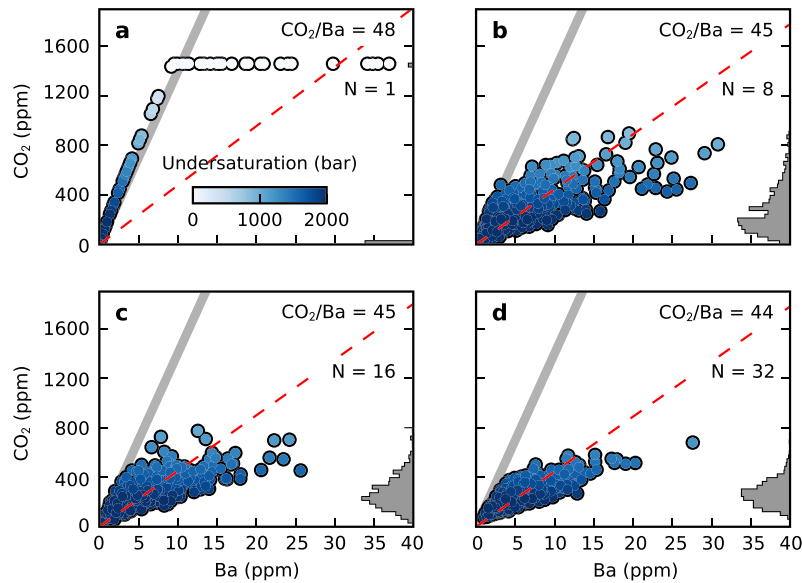


**Fig. B.1.** CO<sub>2</sub>-Ba systematics resulting from varying mixing parameter, and degassing at 2000 bar. As mixing parameter increases, the array condenses towards the depleted melt endmember. Colour indicates CO<sub>2</sub> undersaturation at 2000 bar. See the caption to Fig. 7 for further description.

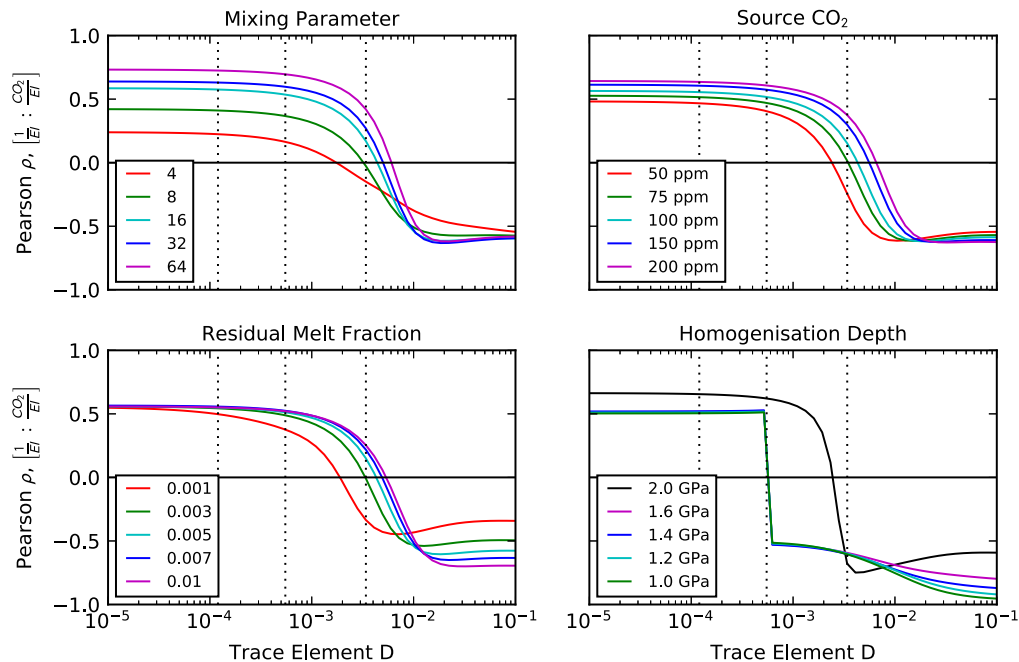


**Fig. C.1.** The effect of variables other than degassing pressure on the Pearson correlation coefficient between 1/EI and CO<sub>2</sub>/EI. Calculations performed at 2000 bar, with other parameters as described in main text, unless noted in the panel key.

homogenisation has taken place. Small amounts of homogenisation do not change the results or conclusions of this paper.

## Appendix B. Effect of mixing parameter on CO<sub>2</sub>-trace element systematics

The effect of the mixing parameter on the distribution of data in CO<sub>2</sub>-trace element space is shown in Fig. B.1. As the mixing parameter increases, the array condenses towards the most depleted melts. A small change in the best fit ratio is seen in Fig. B.1, however this is due to having insufficient draws from the distribution to characterise the mean ratio accurately. As the number of analyses increases the best fit ratio will tend towards the mean ratio, regardless of mixing parameter. The smaller the degree of mixing, the more likely it is for the mantle CO<sub>2</sub>/Ba ratio to be preserved, shown by the number of points lying on the grey line in Fig. B.1. The general systematics described in the main text are not affected by small changes in the mixing parameter. Estimates of the minimum number of analyses required to observe mantle CO<sub>2</sub>/Ba ratios (Section 4.3) will be sensitive to this however, and so these results should be used with care.

## Appendix C. Sensitivity of Pearson correlation coefficient to other parameters

As described in the main text, degassing has a dramatic effect on the behaviour of the Pearson correlation coefficient between CO<sub>2</sub>/El and 1/El, moving the change from positive to negative coefficient towards higher trace element partition coefficient. The pressure at which degassing takes place is a major control on where this transition happens, and the magnitude of the correlation coefficients either side. These properties of the correlation coefficient are not controlled uniquely by degassing pressure however, Fig. C.1 demonstrates how the mixing parameter, source CO<sub>2</sub> concentration, the residual porosity during melting and homogenisation during transport (Appendix A), affects the behaviour of the correlation coefficient. Plots of this type are therefore useful for qualitatively identifying the presence of degassing, but cannot be used to extract degassing pressure quantitatively.

## References

- Bianchi, D., Sarmiento, J.L., Gnanadesikan, A., Key, R.M., Schlosser, P., Newton, R., 2010. Low helium flux from the mantle inferred from simulations of oceanic helium isotope data. *Earth Planet. Sci. Lett.* 297, 379–386.
- Bottinga, Y., Javoy, M., 1990. Mid-ocean ridge basalt degassing: bubble nucleation. *J. Geophys. Res.*, Solid Earth 95 (B4), 5125–5131.
- Boudier, F., Nicolas, A., Ildefonse, B., 1996. Magma chambers in the Oman ophiolite: fed from the top and the bottom. *Earth Planet. Sci. Lett.* 144, 239–250.
- Brown, P.J., Fuller, W.A., 1990. Statistical Analysis of Measurement Error Models and Applications: Proceedings of the AMS–IMS–SIAM Joint Summer Research Conference Held June 10–16, 1989, with Support from the National Science Foundation and the US Army Research Office. American Mathematical Soc.
- Cartigny, P., Pineau, F., Aubaud, C., Javoy, M., 2008. Towards a consistent mantle carbon flux estimate: insights from volatile systematics (H<sub>2</sub>O/Ce, δD, CO<sub>2</sub>/Nb) in the North Atlantic mantle (14 N and 34 N). *Earth Planet. Sci. Lett.* 265, 672–685.
- Craig, H., Clarke, W.B., Beg, M.A., 1975. Excess <sup>3</sup>He in deep water on the East Pacific Rise. *Earth Planet. Sci. Lett.* 26, 125–132.
- Dasgupta, R., 2013. Ingassing, storage, and outgassing of terrestrial carbon through geologic time. *Rev. Mineral. Geochem.* 75, 183–229.
- Dasgupta, R., Hirschmann, M.M., 2010. The deep carbon cycle and melting in Earth's interior. *Earth Planet. Sci. Lett.* 298, 1–13.
- Dixon, E.J., Stolper, E.M., Holloway, J.R., 1995. An experimental study of water and carbon dioxide solubilities in mid-ocean ridge basaltic liquids. Part I: calibration and solubility models. *J. Petrol.* 36, 1607–1631.
- Eguchi, J., Dasgupta, R., 2017. CO<sub>2</sub> content of andesitic melts at graphite-saturated upper mantle conditions with implications for redox state of oceanic basalt source regions and remobilization of reduced carbon from subducted eclogite. *Contrib. Mineral. Petrol.* 172, 12.
- Ghiorso, M.S., Hirschmann, M.M., Reiners, P.W., Kress, V.C., 2002. The pMELTS: a revision of MELTS for improved calculation of phase relations and major element partitioning related to partial melting of the mantle to 3 GPa. *Geochem. Geophys. Geosyst.* 3, 1–35. <http://dx.doi.org/10.1029/2001GC000217>.
- Hauri, E., Gronvold, K., Oskarsson, N., McKenzie, D., 2002. Abundance of carbon in the Icelandic mantle: constraints from melt inclusions. In: AGU Spring Meeting Abstracts, p. 3.
- Hayes, J.M., Waldbauer, J.R., 2006. The carbon cycle and associated redox processes through time. *Philos. Trans. R. Soc. Lond. B, Biol. Sci.* 361, 931–950.
- Helo, C., Longpré, M.-A., Shimizu, N., Clague, D.A., Stix, J., 2011. Explosive eruptions at mid-ocean ridges driven by CO<sub>2</sub>-rich magmas. *Nat. Geosci.* 4, 260–263.
- Herzberg, C., 2004. Partial crystallization of mid-ocean ridge basalts in the crust and mantle. *J. Petrol.* 45, 2389–2405.
- Hirschmann, M.M., Dasgupta, R., 2009. The H/C ratios of Earth's near-surface and deep reservoirs, and consequences for deep Earth volatile cycles. *Chem. Geol.* 262, 4–16.
- Hirschmann, M.M., Stolper, E.M., 1996. A possible role for garnet pyroxenite in the origin of the “garnet signature” in MORB. *Contrib. Mineral. Petrol.* 124, 185–208.
- Jackson, D.A., Somers, K.M., 1991. The spectre of “spurious” correlations. *Oecologia* 86, 147–151.
- Javoy, M., Pineau, F., 1991. The volatiles record of a “popping” rock from the Mid-Atlantic Ridge at 14 N: chemical and isotopic composition of gas trapped in the vesicles. *Earth Planet. Sci. Lett.* 107, 598–611.
- Jian, H., Chen, Y.J., Singh, S.C., Li, J., Zhao, M., Ruan, A., Qiu, X., 2017. Seismic structure and magmatic construction of crust at the ultraslow-spreading Southwest Indian Ridge at 50°28'E. *J. Geophys. Res.*, Solid Earth 122, 18–42.
- Jones, E., Oliphant, T., Peterson, P., 2014. {SciPy}: Open Source Scientific Tools for {Python}.
- Kasting, J.F., Whitmire, D.P., Reynolds, R.T., 1993. Habitable zones around main sequence stars. *Icarus* 101, 108–128.
- Katz, R.F., Spiegelman, M., Langmuir, C.H., 2003. A new parameterization of hydrous mantle melting. *Geochem. Geophys. Geosyst.* 4.
- Kelemen, P.B., Hirth, G., Shimizu, N., Spiegelman, M., Dick, H.J., 1997a. A review of melt migration processes in the adiabatically upwelling mantle beneath oceanic spreading ridges. *Philos. Trans. R. Soc., Math. Phys. Eng. Sci.* 355, 283–318.
- Kelemen, P.B., Koga, K., Shimizu, N., 1997b. Geochemistry of gabbro sills in the crust-mantle transition zone of the Oman ophiolite: implications for the origin of the oceanic lower crust. *Earth Planet. Sci. Lett.* 146, 475–488.
- Kelemen, P.B., Manning, C.E., 2015. Reevaluating carbon fluxes in subduction zones, what goes down, mostly comes up. *Proc. Natl. Acad. Sci.* 112, E3997–E4006.
- Klein, Emily M., Langmuir, Charles H., 1987. Global correlations of ocean ridge basalt chemistry with axial depth and crustal thickness. *J. Geophys. Res.*, Solid Earth 92 (B8), 8089–8115.
- Le Voyer, M., Kelley, K.A., Cottrell, E., Hauri, E.H., 2017. Heterogeneity in mantle carbon content from CO<sub>2</sub>-undersaturated basalts. *Nat. Commun.* 8, 14062.
- Lundstrom, C.C., Sampson, D.E., Perfit, M.R., Gill, J., Williams, Q., 1999. Insights into mid-ocean ridge basalt petrogenesis: U-series disequilibria from the Siqueiros Transform, Lamont Seamounts, and East Pacific Rise. *J. Geophys. Res.*, Solid Earth 104, 13035–13048.
- MacLennan, J., 2008. Concurrent mixing and cooling of melts under Iceland. *J. Petrol.* 49, 1931–1953.
- MacLennan, J., McKenzie, D., Gronvold, K., Slater, L., 2001. Crustal accretion under northern Iceland. *Earth Planet. Sci. Lett.* 191, 295–310.
- MacLennan, J., McKenzie, D., Gronvold, K., Shimizu, N., Eiler, J.M., Kitchen, N., 2003. Melt mixing and crystallization under Theistareykir, northeast Iceland. *Geochem. Geophys. Geosyst.* 4, 8624.
- Marty, B., 2012. The origins and concentrations of water, carbon, nitrogen and noble gases on Earth. *Earth Planet. Sci. Lett.* 313, 56–66.
- Matthews, S., Shorttle, O., MacLennan, J., 2016. The temperature of the Icelandic mantle from olivine-spinel aluminum exchange thermometry. *Geochem. Geophys. Geosyst.* 17, 4725–4752.
- McKenzie, D., O'Nions, R.K., 1991. Partial Melt Distributions from Inversion of Rare Earth Element Concentrations. *J. Petrol.* 32, 1021–1091.
- McKenzie, D., O'Nions, R.K., 1995. The Source Regions of Ocean Island Basalts. *J. Petrol.* 36, 133–159.
- Michael, P.J., Graham, D.W., 2015. The behavior and concentration of CO<sub>2</sub> in the suboceanic mantle: inferences from undegassed ocean ridge and ocean island basalts. *Lithos* 236, 338–351. <http://dx.doi.org/10.1016/j.lithos.2015.08.020>.
- Moore, J.G., 1979. Vesicularity and CO<sub>2</sub> in mid-ocean ridge basalt. *Nature* 282, 250–253.
- Neave, D.A., Putirka, K.D., 2017. A new clinopyroxene-liquid barometer, and implications for magma storage pressures under Icelandic rift zones. *Am. Mineral.* 102, 777–794.
- Perfit, M.R., Fornari, D.J., Ridley, W.I., Kirk, P.D., Casey, J., Kastens, K.A., Reynolds, J.R., Edwards, M., Desonie, D., Shuster, R., 1996. Recent volcanism in the Siqueiros transform fault: picritic basalts and implications for MORB magma genesis. *Earth Planet. Sci. Lett.* 141, 91–108.
- Resing, J.A., Lupton, J.E., Feely, R.A., Lilley, M.D., 2004. CO<sub>2</sub> and <sup>3</sup>He in hydrothermal plumes: implications for mid-ocean ridge CO<sub>2</sub> flux. *Earth Planet. Sci. Lett.* 226, 449–464.
- Rosenthal, A., Hauri, E.H., Hirschmann, M.M., 2015. Experimental determination of C, F, and H partitioning between mantle minerals and carbonated basalt, CO<sub>2</sub>/Ba

- and CO<sub>2</sub>/Nb systematics of partial melting, and the CO<sub>2</sub> contents of basaltic source regions. *Earth Planet. Sci. Lett.* 412, 77–87. <http://dx.doi.org/10.1016/j.epsl.2014.11.044>.
- Rudge, J.F., MacLennan, J., Stracke, A., 2013. The geochemical consequences of mixing melts from a heterogeneous mantle. *Geochim. Cosmochim. Acta* 114, 112–143.
- Saal, A.E., Hauri, E.H., Langmuir, C.H., Perfit, M.R., 2002. Vapour undersaturation in primitive mid-ocean-ridge basalt and the volatile content of Earth's upper mantle. *Nature* 419, 451–455. <http://dx.doi.org/10.1038/nature01073>.
- Shaw, A.M., Behn, M.D., Humphris, S.E., Sohn, R.A., Gregg, P.M., 2010. Deep pooling of low degree melts and volatile fluxes at the 85 E segment of the Gakkel Ridge: evidence from olivine-hosted melt inclusions and glasses. *Earth Planet. Sci. Lett.* 289, 311–322.
- Shimizu, K., Saal, A.E., Myers, C.E., Nagle, A.N., Hauri, E.H., Forsyth, D.W., Kamenetsky, V.S., Niu, Y., 2016. Two-component mantle melting–mixing model for the generation of mid-ocean ridge basalts: implications for the volatile content of the Pacific upper mantle. *Geochim. Cosmochim. Acta* 176, 44–80. <http://dx.doi.org/10.1016/j.gca.2015.10.033>.
- Shishkina, T.A., Botcharnikov, R.E., Holtz, F., Almeev, R.R., Jazwa, A.M., Jakubiak, A.A., 2014. Compositional and pressure effects on the solubility of H<sub>2</sub>O and CO<sub>2</sub> in mafic melts. *Chem. Geol.* 388, 112–129.
- Shorttle, O., Rudge, J.F., MacLennan, J., Rubin, K.H., 2016. A statistical description of concurrent mixing and crystallization during MORB differentiation: implications for trace element enrichment. *J. Petrol.* 57, 2127–2162.
- Smith, P.M., Asimow, P.D., 2005. Adibat\_1ph: a new public front-end to the MELTS, pMELTS, and pHMELTS models. *Geochem. Geophys. Geosyst.* 6. <http://dx.doi.org/10.1029/2004GC000816>.
- Sobolev, A.V., 1996. Melt inclusions in minerals as a source of principle petrological information. *Petrology* 4, 209–220.
- Sobolev, A.V., Gurenko, A.A., Shimizu, N., 1994. Ultra-depleted melts from Iceland: data from melt inclusion studies. *Miner. Mag. A* 58, 860–861.
- Spiegelman, M., Kelemen, P.B., 2003. Extreme chemical variability as a consequence of channelized melt transport. *Geochem. Geophys. Geosyst.* 4.
- Walker, J.C.G., Hays, P.B., Kasting, J.F., 1981. A negative feedback mechanism for the long-term stabilization of Earth's surface temperature. *J. Geophys. Res., Oceans* 86, 9776–9782.
- Wanless, V.D., Behn, M.D., Shaw, A.M., Plank, T., 2014. Variations in melting dynamics and mantle compositions along the Eastern Volcanic Zone of the Gakkel Ridge: insights from olivine-hosted melt inclusions. *Contrib. Mineral. Petrol.* 167, 1–22.
- Winpenny, B., MacLennan, J., 2011. A partial record of mixing of mantle melts preserved in Icelandic phenocrysts. *J. Petrol.* 52, 1791–1812.
- Workman, R.K., Hart, S.R., 2005. Major and trace element composition of the depleted MORB mantle (DMM). *Earth Planet. Sci. Lett.* 231, 53–72.
- Zou, H., 2007. *Quantitative Geochemistry*. World Scientific.